THE EUROPEAN ORGANIZATION FOR NUCLEAR RESEARCH

OPTIMIZATION AND PRODUCTION OF INTERCONNECTION BOX FOR ATLAS – HGTD

CERN Summer Student Program 2024 Project Report

Prepared by

Merve Sude ALKAN

Supervised by

Stefan GUINDON

Department

ATLAS - HGTD

Date

28/09/2024

Abstract

The High-Granularity Timing Detector (HGTD) is a cutting-edge technology developed for the ATLAS experiment at CERN's Large Hadron Collider (LHC), as part of the Phase II upgrade. Its key purpose is to provide highly precise time measurements at the picosecond level, which aids in more accurate reconstruction of events by distinguishing between particle collisions that occur in quick succession. This capability is especially beneficial in high-luminosity environments, helping to minimize the effects of pile-up, where numerous proton-proton interactions happen simultaneously within the same event.

HGTD will be installed in ATLAS detector during the Long Shutdown 3 (LS3) of the LHC. Specifically, it will be positioned in the forward region of the ATLAS detector, located between the calorimeters and the inner tracker. This region is very close to the interaction point where particle collisions occur.

As part of the HGTD project, this report focuses on the optimization and production of the interconnection box designed to connect a set of pipes to other parts in the HGTD, the heat transfer analysis for the pipe carrying nitrogen gas and passing through the interconnection box. Additionally, as a side project, the report includes the production of different types of materials to be used in R&D projects for sensors at CERN.

Keywords: ATLAS, HGTD, Excel, CAD, Siemens NX, 3D Printing, Manufacturing, Heat Transfer

Acknowledgements

I would like to express my sincere gratitude to my supervisor, Stefan Guindon, for all the support, guidance, and kindness he provided throughout my internship, as his invaluable assistance and encouragement have greatly contributed to my personal and professional growth. I also extend my heartfelt thanks to Aboud Falou for his contributions to my project and the valuable knowledge he taught me in mechanical engineering, which have been instrumental in my development. Additionally, I am grateful to Torsten Koettig from the Central Cryogenic Laboratory for his assistance with my heat transfer analysis task; his support has significantly enhanced my understanding of the subject. Finally, I thank Dominik Dannheim for serving as a bridge between the EP-DT-TP department and the HGTD department for my two separate tasks, as his coordination has been crucial for the success of my work.

Lastly, I would like to express my appreciation to the entire HR team, especially Tereza Veselá and Anastasija Preobrazenska for their support throughout the program; their assistance has been incredibly important to me.

Contents

1. Introduction

The project is divided into three sub-projects. The first sub-project involves observing the manufacturing process of the interconnection box developed for HGTD and ultimately producing a prototype of this box. The aim is to produce a prototype of the interconnection box using 3D printing, due to the difficulties in manufacturing arising from differences in its design, and to make necessary adjustments based on the prototype before producing the final version.

The second sub-project focuses on conducting a heat transfer analysis for the nitrogen-carrying pipe within the interconnection box. This includes observing the variations in other properties based on temperature and determining whether the magnitude of the flow rate, pipe length, and other parameters is sufficient.

The last sub-project, carried out separately from the others, covers the research, development, and production through 3D printing of materials used in ENIG (Electroless Nickel Immersion Gold) plating of chips, which are used in CERN R&D projects, carried out by the EP-DT-TP department.

In the report, the first two sub-projects are grouped under the main project titled *Optimization and Production of the Interconnection Box*, while the final sub-project is considered as an extra task and addressed under the title *Production of Materials for ENIG Plating*.

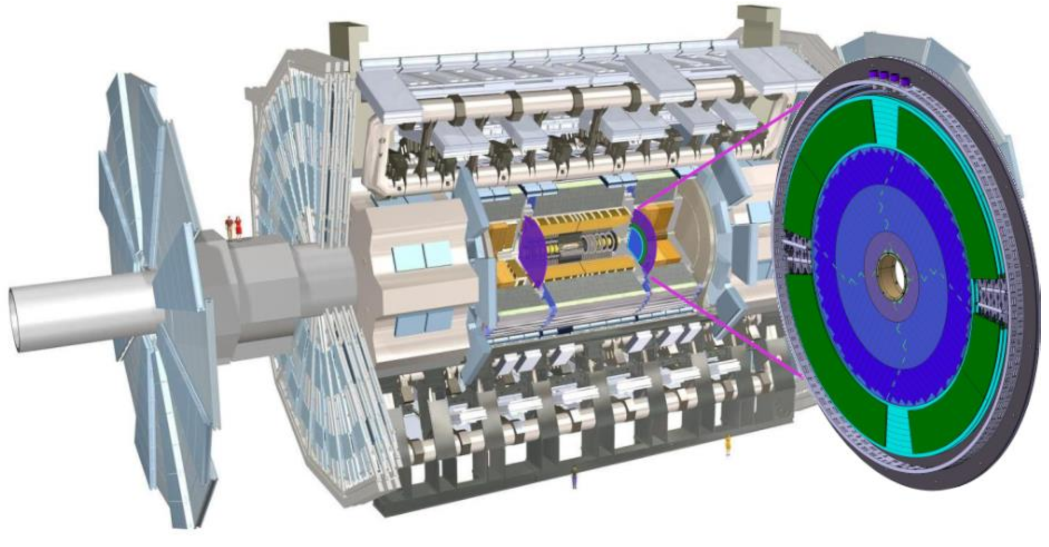

Figure 1: Position of the HGTD within the ATLAS Detector.

2. Optimization and Production of the Interconnection Box

2.1 Production of Interconnection Box

2.1.1 Introduction

The interconnection box plays a crucial role within the HGTD. It acts as a bridge for transferring the pipes carrying liquid CO_2 used for cooling and the pipes carrying dry nitrogen. Various models of this box have been previously produced, but issues were encountered with its design. This report addresses the production of a prototype for the latest design, known as the "Green Box," which was created by making modifications to the earlier designs.

First, the prototype of the previous version was disassembled and examined.

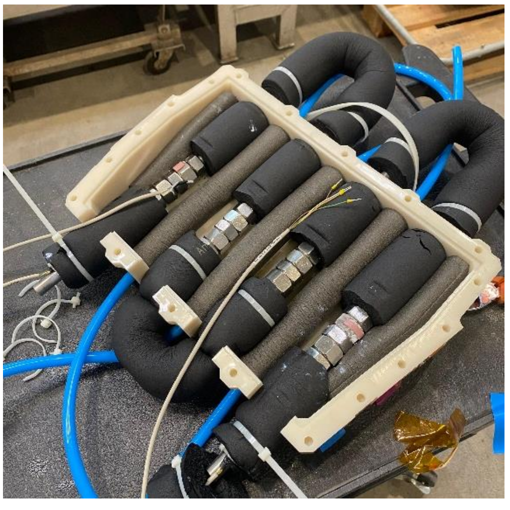

Figure 2.1.1: Assembled prototype of the previous version of the box.

Figure 2.1.2: Semi-disassembled box

In Figure 2.1.1, the blue pipes represent the thinner pipes carrying nitrogen gas, while the other pipes represent those carrying liquid CO_2 used for cooling. In Figure 2.1.2, the CO_2 pipes can be observed in more detail.

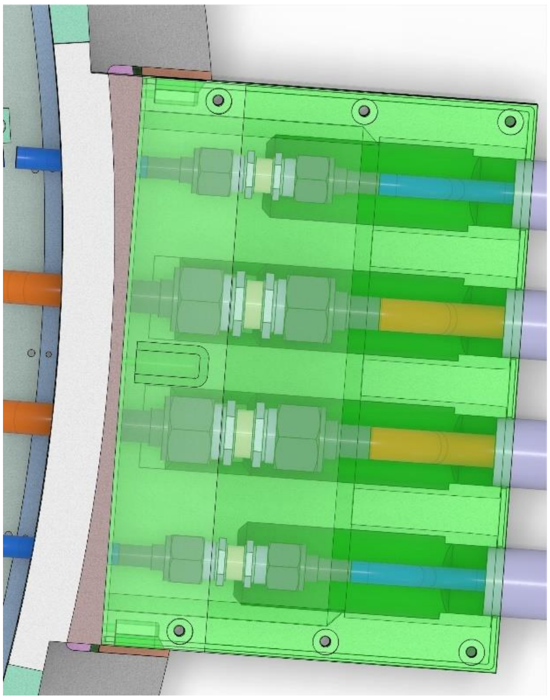

Figure 2.1.3: Front view of Green Box

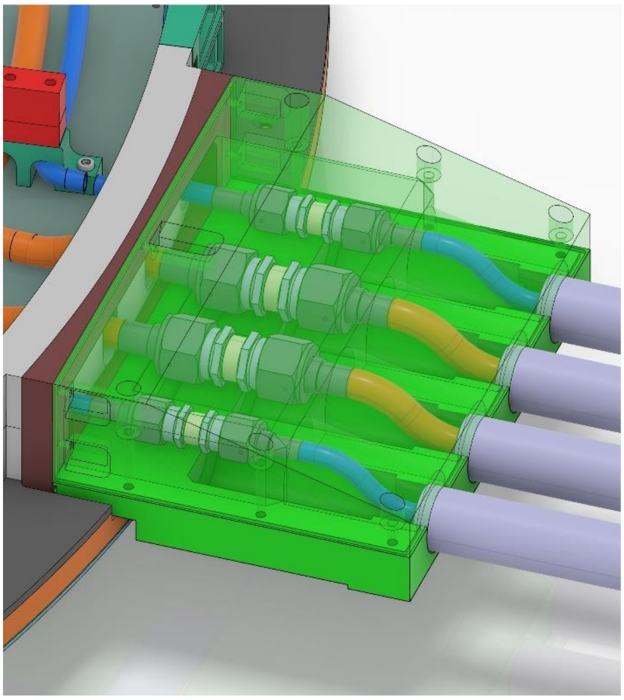

Figure 2.1.4: General view of Green Box

In Figure 2.1.3 and Figure 2.1.4 the 3D model of the new version of the interconnection box which is called Green Box can be examined. The blue pipes again represent the pipes carrying dry nitrogen.

2.1.2 Production

To produce the Green Box, various options must be identified, and one must be selected. The primary challenge is optimizing the density for 3D printing. We require a thermally shielded box. To enhance thermal shielding, a low density is preferred, but a higher density is necessary to increase mechanical stiffness. The final material for this interconnection box will be either PEEK or ULTEM due to their radiation hardness. The cost of the raw material may vary depending on the process applied, whether 3D printing or milling. 3D printing presents the best compromise between raw material cost and the conformity of the box to its original specifications.

For 3D Printing, Prusa i3 MK3 model 3D printing machine has been used.

The prototype filament used was PLA Silver, but there were two versions of this filament: one original and the other commercial. It was observed that the original filament had to be used instead of the commercial version due to issues that hindered the 3D printing process. Despite these challenges, by adding support around the box and switching to the original filament, the printing was ultimately completed successfully

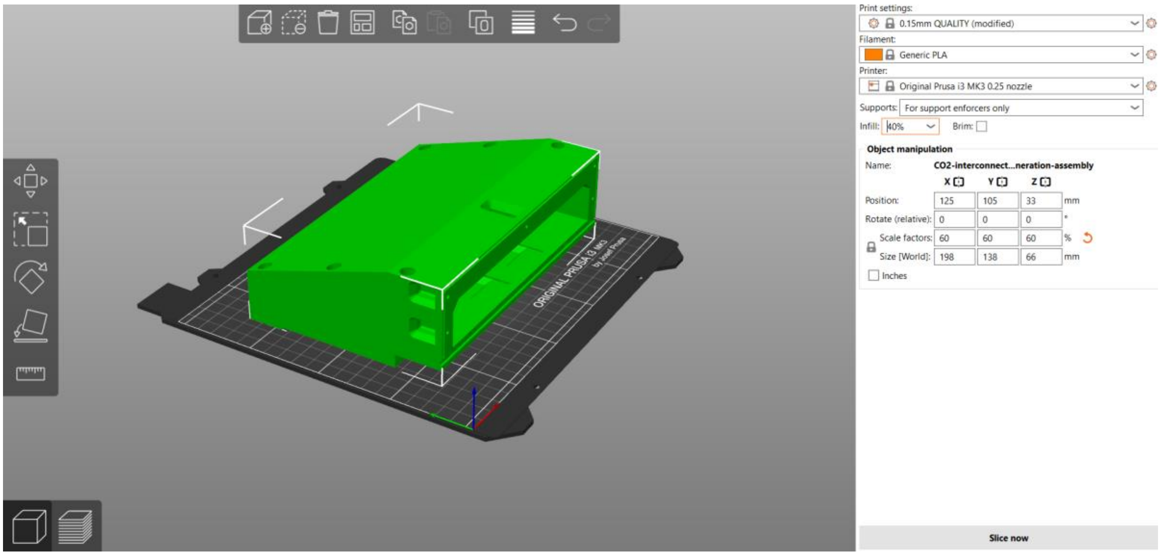

Figure 2.1.5: The 3D Printing application of Prusa, with the specified options for Green Box

In Figure 2.1.5, it can be observed that the required density is approximately 40%. Due to the limited size of the 3D printing machine, the scale can be a maximum of 60% of the actual design size. Finally, the necessary support has been added.

Figure 2.1.6: Side view of 3D printed version of Green Box.

Figure 2.1.7: General view of 3D printed version of Green Box.

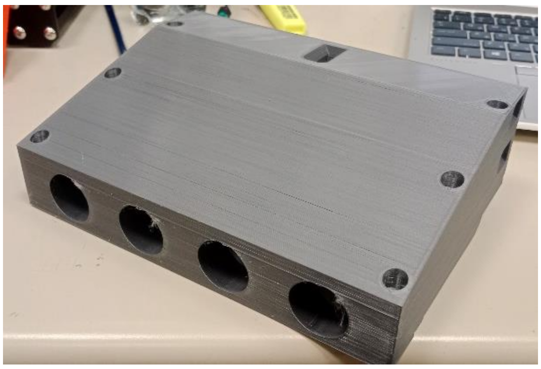

Figure 2.1.8: Back view of 3D printed version of Green Box

2.2 Heat Transfer Analysis for Dry Nitrogen

2.2.1 Introduction

The HGTD hermetic vessel shall be purged with dry nitrogen to prevent condensation on the detector components. For gas circulation, each vessel shall be fitted with an inlet pipe and an outlet pipe with an inner diameter of 16 mm and 14 mm respectively.

As mentioned above, the interconnection box includes pipes carrying dry nitrogen. These pipes need to be examined as they transition from the cooler part to the hotter part in the HGTD. The temperature at the beginning of the pipe is -35 ℃, which increases as the gas flows through the pipe, ultimately reaching the ambient temperature of 20 ℃. The objective of this task is to observe the change in characteristics of the properties along with the change in temperature and indicate whether the specified values for the pipe and the gas are adequate and accurate.

Due to the limited time available for this task, it is assumed that the temperature increases linearly with the length of the pipe to simplify the calculations. While this may not accurately reflect real-life applications, this assumption was made solely to observe and understand the general behaviors of the properties as the temperature increases.

For the calculations and plots, Excel had been used.

2.2.2 Calculations

The predetermined values given for use in calculations

Properties	**Values**
Gas	N_2
Outer Diameter	D_o = 16 mm
Length of Pipe	L = 3.5 m
Inlet Temperature	$T_i = 238\,K$
Outlet Temperature	$T_o = 293\,K$
Thickness of Pipe	$t = 1\,mm$
Pipe Material	$SS\ 316\ L$
Pressure	$p = 1\,bar$

Temperature increases linearly along with the length. So in each 63.6363 mm, 1℃ increase in temperature happens.

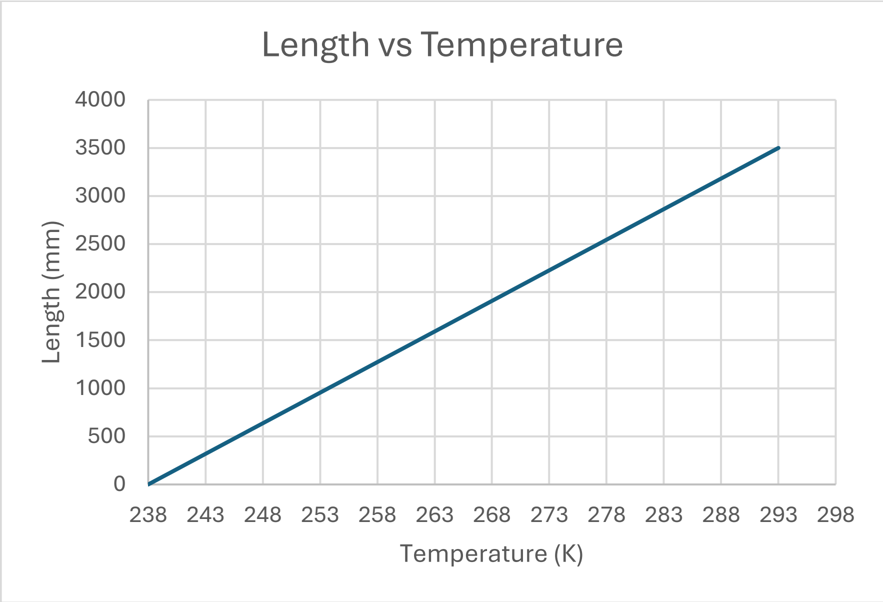

Figure 2.2.1: Graph of Length vs Temperature.

Three different volumetric flow rate values were determined to observe the variations in data.

$\dot{V}$ $in\ L/min$	$\dot{V}$ $in\ L/s$
150	2,5
120	2
50	0,83333333

As the temperature changes, the values of c_p (specific heat capacity), density, thermal conductivity coefficient λ, and dynamic viscosity μ also vary with temperature. These parameter values were interpreted from the data provided by the Central Cryogenic Laboratory. The constant used to obtain these values was pressure, set at 1 bar.

Mass flow rates for each volumetric flow rate have been found by multiplying volumetric flow rate and density.

$$\dot{V}\left(\frac{L}{s}\right) \times \rho\ (\frac{kg}{m^3}) = \dot{m}\ \left(\frac{g}{s}\right)$$

The heat flow rate in each 1°C change is found by the equation:

$$\dot{m}\left(\frac{g}{s}\right) \times c_p(\frac{J}{gK}) \times \Delta T(K) = \dot{Q}(W)$$

For each calculation, $\Delta T = 1$, and for the $\dot{m}$ and c_p values, the average of two points' values are calculated.

=(Q3+Q2)/2*(N3+N2)/2+V2

N	O	P	Q	R	S	T	U	V	W	X
cp in J/gK	Density	5.78 mass	2.5 mass fl	2 mass flo	0.83333 masss flow		Q_dot in W	Q_dot in W	Q_dot in W	Q_dot in W
1,042	1,4171	8,190838	3,54275	2,8342	1,180916		0	0	0	0
1,042	1,4111	8,156158	3,52775	2,8222	1,175916		8,516785	3,683731	2,946984	1,22791
1,0419	1,4052	8,122056	3,513	2,8104	1,171		16,99733	7,351785	5,881428	2,450594
1,0419	1,3994	8,088532	3,4985	2,7988	1,166166		25,44223	11,00443	8,803541	3,668141
1,0419	1,3935	8,05443	3,48375	2,787	1,16125		33,85191	14,64183	11,71346	4,880608
1,0419	1,3878	8,021484	3,4695	2,7756	1,1565		42,22666	18,26412	14,6113	6,088039
1,0418	1,3821	7,988538	3,45525	2,7642	1,15175		50,56668	21,8714	17,49712	7,290464
1,0418	1,3764	7,955592	3,441	2,7528	1,147		58,87197	25,46366	20,37093	8,487882
1,0418	1,3708	7,923224	3,427	2,7416	1,142333		67,14325	29,0412	23,23296	9,680395
1,0418	1,3652	7,890856	3,413	2,7304	1,137666		75,3808	32,60415	26,08332	10,86805
1,0418	1,3597	7,859066	3,39925	2,7194	1,133083		83,58494	36,15266	28,92212	12,05088

Figure 2.2.2: Calculation of heat flow rate.

In the end, all $\dot{Q}$ values in each cell are summed up and the required $\dot{Q}$ value for the whole flow is found.

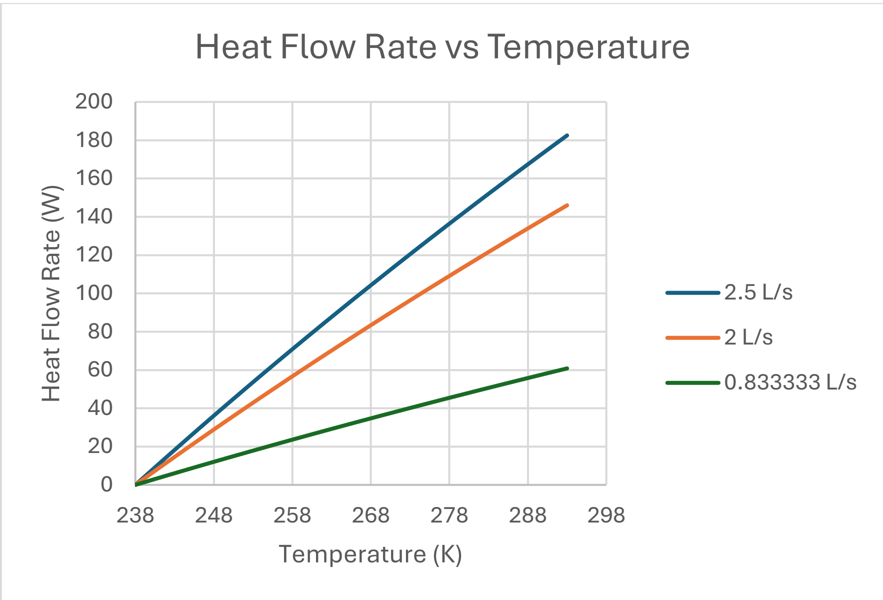

Figure 2.2.3: Total Heat Flow Rate vs Temperature

To find the $\dot{Q}$, supplied from the outside of the tube, first the convection heat transfer coefficient, α, should be found.

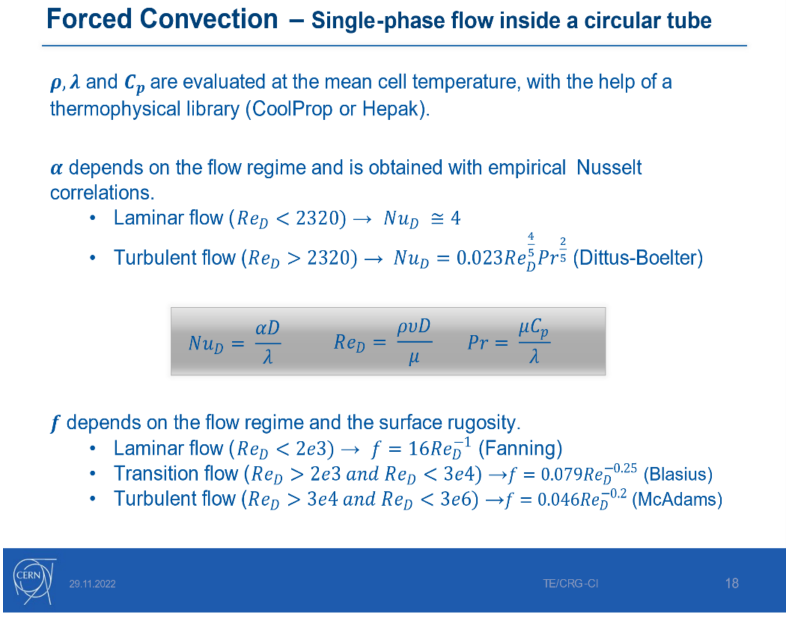

Figure 2.2.4: Equations for Nu_D, Re_D and Pr.

To obtain the α value, the Reynolds number, Re_D, in each cell must first be calculated. Based on the Re_D value, the flow regime should then be determined.

In Figure 2.2.3, D value equals inner diameter, which equals $D_o - 2t = 14\ mm$.

v value is the velocity (m/s), which equals $\dot{V}\left(\frac{L}{s}\right) \times 10^{-3} \times A\ (m^2)$. A is the cross-sectional area of the inner pipe. $A = \frac{\pi \times 0.014^2}{4} m^2$

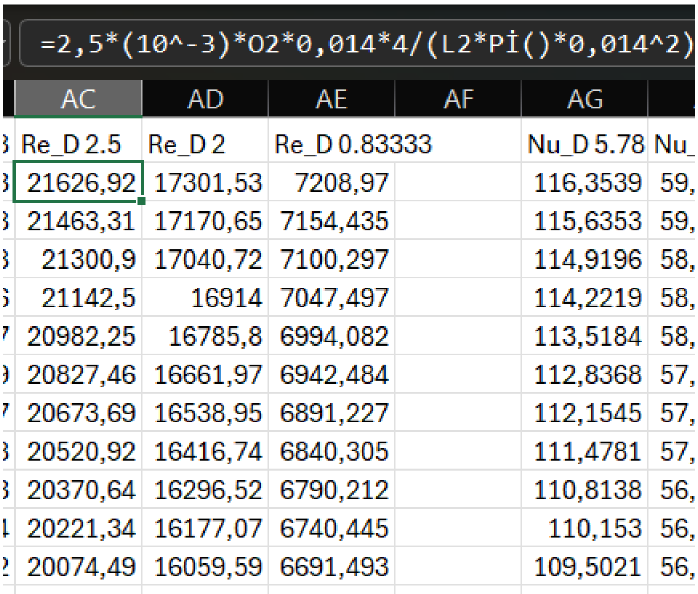

=2,5*(10^-3)*O2*0,014*4/(L2*PI()*0,014^2)

AC	AD	AE	AF	AG	
Re_D 2.5	Re_D 2	Re_D 0.83333		Nu_D 5.78	Nu_
21626,92	17301,53	7208,97		116,3539	59,
21463,31	17170,65	7154,435		115,6353	59,
21300,9	17040,72	7100,297		114,9196	58,
21142,5	16914	7047,497		114,2219	58,
20982,25	16785,8	6994,082		113,5184	58,
20827,46	16661,97	6942,484		112,8368	57,
20673,69	16538,95	6891,227		112,1545	57,
20520,92	16416,74	6840,305		111,4781	57,
20370,64	16296,52	6790,212		110,8138	56,
20221,34	16177,07	6740,445		110,153	56,
20074,49	16059,59	6691,493		109,5021	56,

Figure 2.2.5: Reynolds Number Calculation.

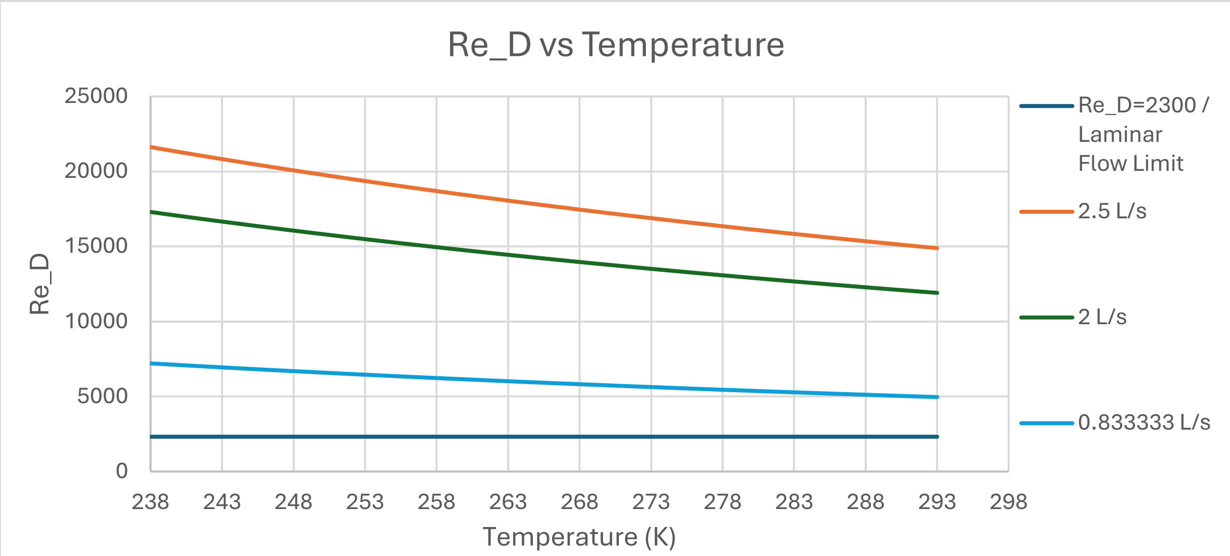

Figure 2.2.6: Graph of Re_Dvs Temperature.

Considering Figure 2.2.5, the Re_D value for each volumetric flow rate is always above 2320. Which means the flow regime is always turbulent for all volumetric flow rate temperature values.

From this, it can be inferred that the subsequent calculations will be based on turbulent flow. According to Figure 2.2.3, the Prandtl number, Pr, must first be determined to calculate the applicable formula.

To find Pr for each cell, the interpreted values, μ, λ and c_p are used.

$$Pr = \frac{\mu\ (Pa \times s) \times 10^{-3} \times c_P\left(\frac{J}{gK}\right)}{\lambda\left(\frac{W}{mK}\right)}$$

Finally, the Nusselt number, Nu_D values are calculated and the α values for each cell and each volumetric flow rate are found.

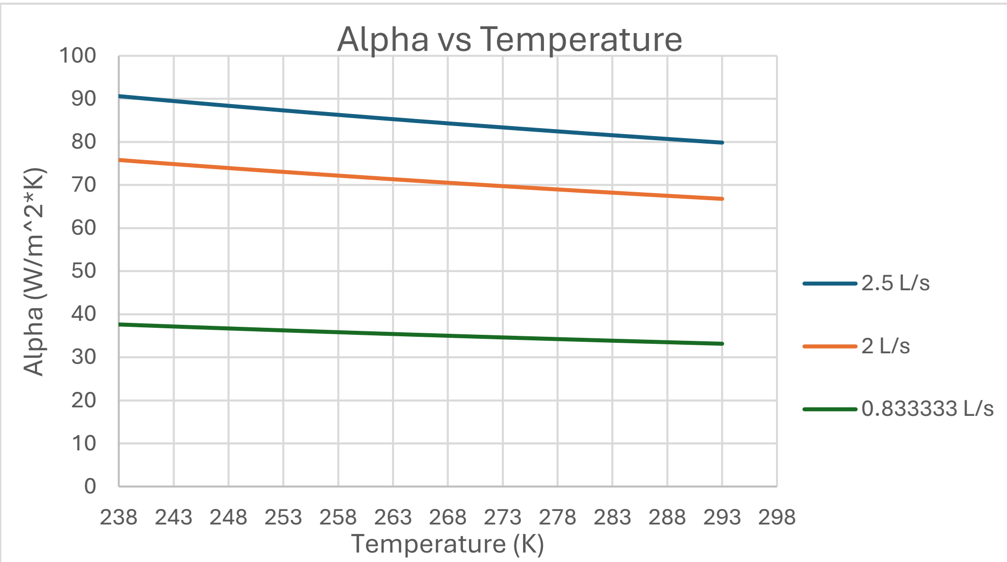

Figure 2.2.7: Graph of α vs Temperature

In the 2nd step, the supplied $\dot{Q}$ values are calculated.

The $\dot{Q}$ values passing through the wall and interface must be equal. Therefore, the equations for these two $\dot{Q}$ values can be equated, resulting in a single equation.

For the wall: $\dot{Q} = \lambda \times \frac{A_{ss}}{l} \times \Delta T_{ss}$ For the interface: $\dot{Q} = \alpha \times A_g \times \Delta T_g$

Here, λ represents the thermal conductivity coefficient of Stainless Steel, which varies with the change in temperature. The equation that is used to find λ values for each cell is provided by Central Cryogenic Labaratory.

A_{ss} equals the tube surface area, $A_{ss} = \pi \times \frac{D_o+D_i}{2} \times l$, $l = cell\ length = 0.06363\ m$

A_g equals the inner tube surface in contact with the dry nitrogen, $A_g = \pi \times D_i \times l$

$l = cell\ length = 0.06363\ m$

ΔT_{ss} is the temperature change through the stainless steel part of the tube, ΔT_g is the temperature change through the dry nitrogen part.

$$\lambda \times \frac{A_{ss}}{l} \times \Delta T_{ss} = \alpha \times A_g \times \Delta T_g$$

$$\rightarrow \alpha \times \pi \times 0.014 \times 0.06363 \times \Delta T_g = \lambda \times \frac{\pi \times 0.015 \times 0.06363}{0.06363} \times \Delta T_{ss} \quad [Eq.1]$$

Here, the α and λ values are known. There are two unknown parameters: ΔT_g and ΔT_{ss}

Since the ambient temperature equals 20℃, the sum of these two parameters in every cell always equals the difference between ambient temperature and instant temperature at the cell.

$$\Delta T_g + \Delta T_{ss} = 293\ K - T_{instant} \rightarrow \Delta T_{ss} = 293 - T_{instant} - c \quad [Eq.2]$$

At this point, only one parameter remains unknown.

By substituting Eq.2 into Eq.1 a new equation is obtained:

$$\Delta T_g = \frac{293 - T_{instant}}{\frac{\alpha}{\lambda} \times \frac{14}{16} \times 0.06363 + 1} \quad [Eq.3]$$

By using Eq.3, $\Delta T_g, \Delta T_{ss}$ and $\dot{Q}$ values for each cell, and total $\dot{Q}$ value supplied are calculated.

To observe the rate of temperature change from the inner part to the outer part of the tube along its length, the temperature values at the contact points for each cell are also determined.

T (K)	dT_fl_2	dT_ss_2	T_contact_	Q_2
238	0	0	238	0
239	40,65917	13,34083	279,6592	10,28689
240	39,95074	13,04926	279,9507	20,36861
241	39,23947	12,76053	280,2395	30,24645
242	38,52738	12,47262	280,5274	39,92018
243	37,8126	12,1874	280,8126	49,39103
244	37,09657	11,90343	281,0966	58,6591
245	36,37833	11,62167	281,3783	67,72525
246	35,65823	11,34177	281,6582	76,5901
247	34,93654	11,06346	281,9365	85,25403
248	34,21278	10,78722	282,2128	93,71784
249	33,48776	10,51224	282,4878	101,9817
250	32,76019	10,23981	282,7602	110,0467

Figure 2.2.8: Calculations for $\Delta T_g, \Delta T_{ss}, T_{contact}$ and $\dot{Q}$ for $\dot{V} = 2\ L/s$

2.2.3 Results

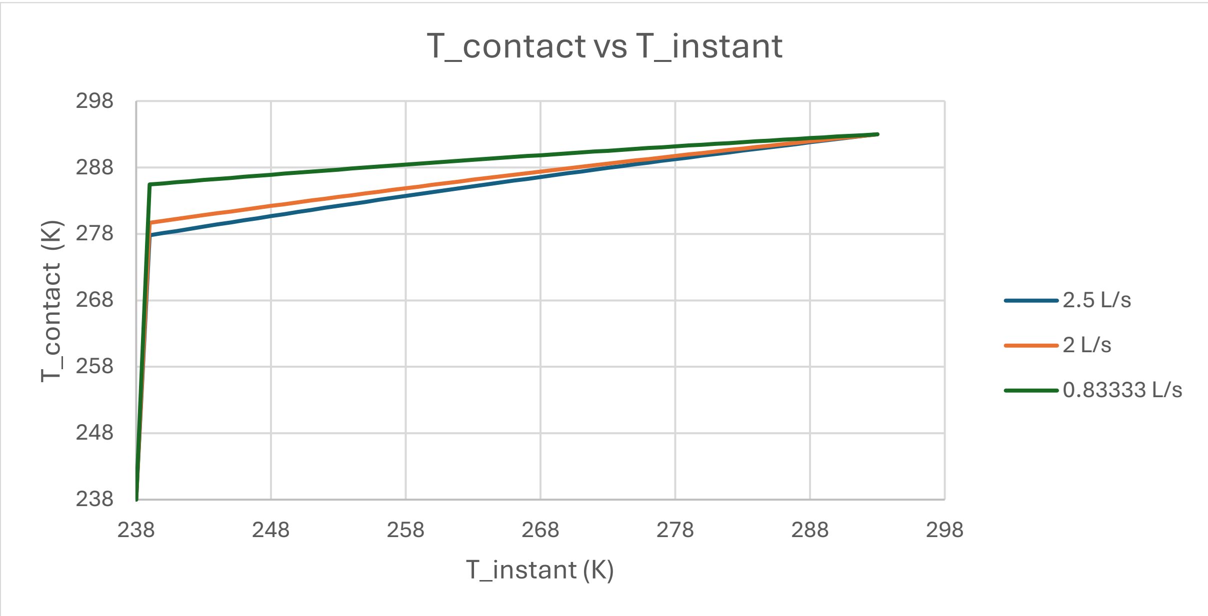

Figure 2.2.9: Graph of $T_{contact}\ vs\ T_{instant}$.

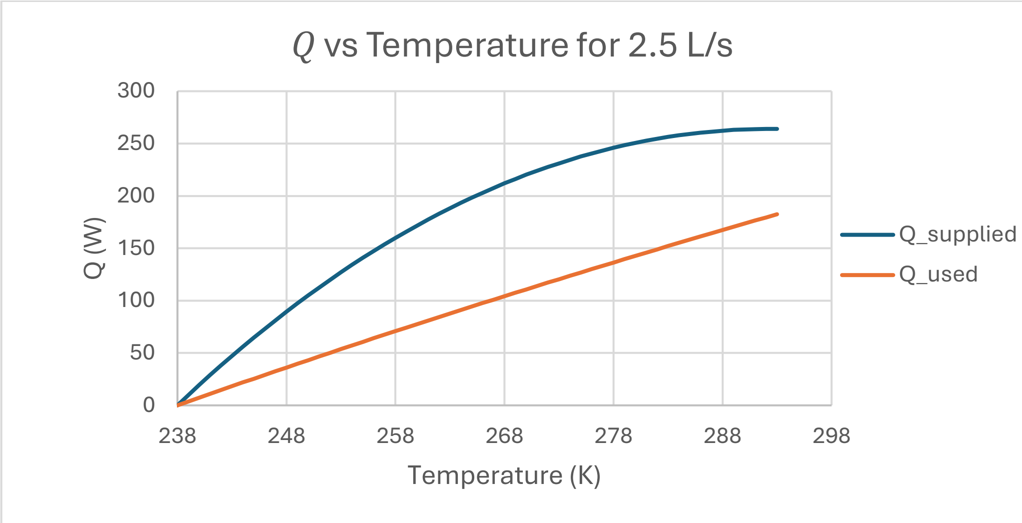

Figure 2.2.10: Graph of $\dot{Q}$ vs Temperature for 2.5 L/s.

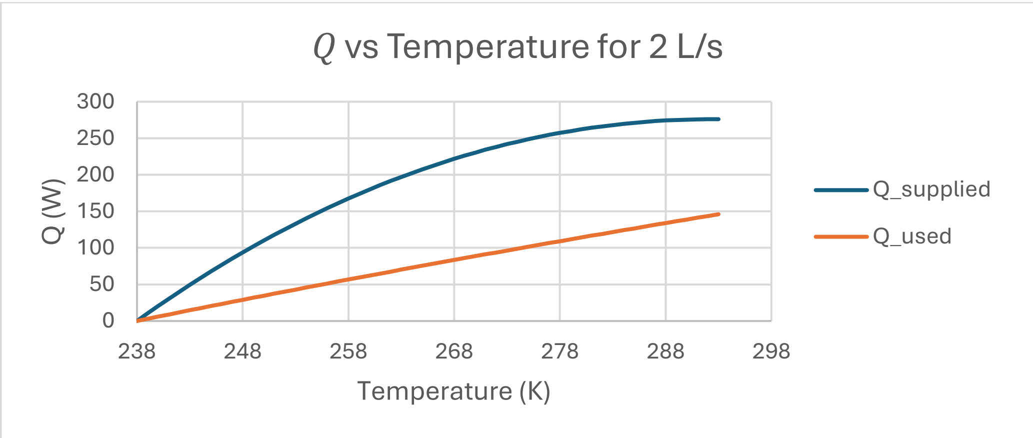

Figure 2.2.11: Graph of $\dot{Q}$ vs Temperature for 2 L/s.

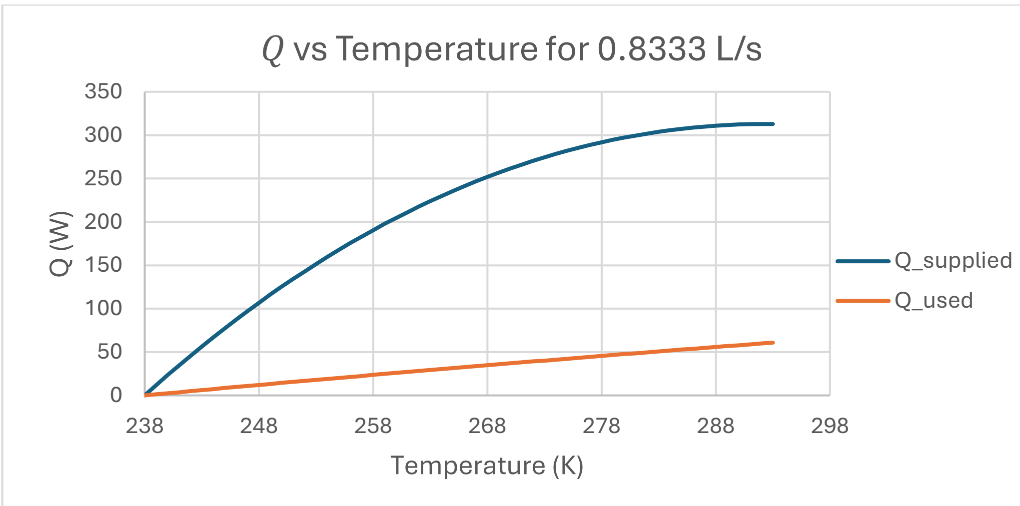

Figure 2.2.12: Graph of $\dot{Q}$ vs Temperature for 0.8333 L/s.

Considering the graphs obtained from the above equations, all volumetric flow rate values satisfy the required $\dot{Q}$ values. It is observed that as the volumetric flow rate increases, the difference between the supplied and used $\dot{Q}$ values decreases. To prevent unnecessary heat supply, the volumetric flow rate can be maintained at higher levels.

As previously discussed, the $T_{contact}$ vs. Length graph is intended to illustrate the results of the assumed linear temperature increase, which is not applicable in a real-life scenario. For this assumption to hold, the heat supplier would need to vary the amount of heat supplied to each cell. In contrast, in reality, heaters provide a constant amount of heat.

Nevertheless, by analyzing the graph, it becomes evident that as the volumetric flow rate increases, the initial jump in temperature change decreases, which is more reasonable. Therefore, selecting a higher volumetric flow rate would be preferable.

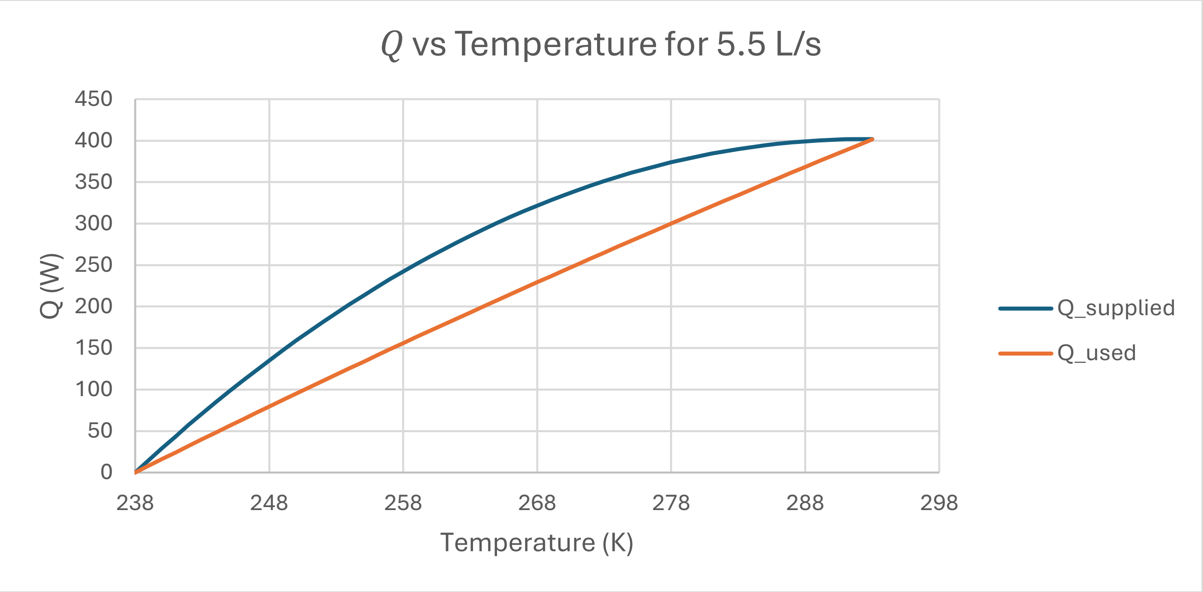

Figure 2.2.13: Graph of $\dot{Q}$ vs Temperature for 5.5 L/s.

In addition to these results, the highest volumetric flow rate that provides sufficient $\dot{Q}$ was determined using the trial-and-error method. At a volumetric flow rate of 5.5 L/s, the supplied and used $\dot{Q}$ values are nearly equal. Beyond this rate, the supplied $\dot{Q}$ is insufficient to further increase the temperature.

Beyond this value, several adjustments to the set-up are required to increase the volumetric flow rate. For instance, the length of the pipe could be extended. However, the maximum specified length for the pipe is 3.5 m, meaning the volumetric flow rate cannot be increased further.

3. Production of Materials for ENIG Plating

3.1 Introduction

ENIG plating, which stands for Electroless Nickel Immersion Gold, is a technique that involves chemical processes and must be applied to the chips used in sensors before they are bonded using the flip-chip method. The primary goal here is to create bumps on the surface of the chips. These bumps assist in connecting the chips during the flip-chip process.

ENIG plating consists of three main stages:

- Pretreatment and zincation of the aluminum pad
- Electroless nickel deposition (formation of the bump)
- Self-catalytic reaction on the pad surface
- Immersion gold (corrosion protection, bondable surface)

The student's objective here is to design holders that will be mounted onto the chips during chemical experiments. Additionally, the student is responsible for designing other necessary components for these experiments. These designs can be categorized as holders, fans, clamps, and lids.

One of the challenging aspects here is that the components are designed at very small scales. These small structures need to be durable. Efforts are being made to produce robust materials using minimal amounts of material. Another consideration is the material used in 3D printing. There are essentially two materials for 3D printing: PP (polypropylene) and PLA (polylactic acid). While PLA is normally a more durable material, it cannot be used specifically for holders and clamps. This is because these components will come into contact with liquids such as zincate and gold during chemical experiments, and they must not react with these substances.

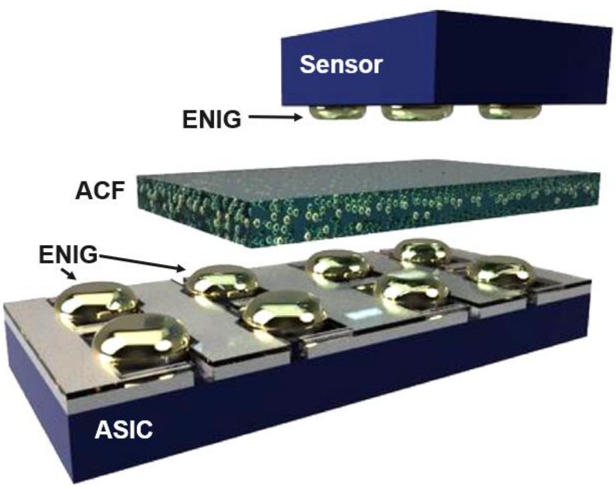

3.2 Design

To mount the chips, a holder; to secure the holders, clamps; to cover the experimental container and to put the clamps on a place, a lid; to evenly distribute the experimental liquid within the container, two different fans were developed for this project. The designs were created using Siemens NX. To ensure compatibility of the designs with the chips, measurements of the previous holders and chips were taken using a caliper.

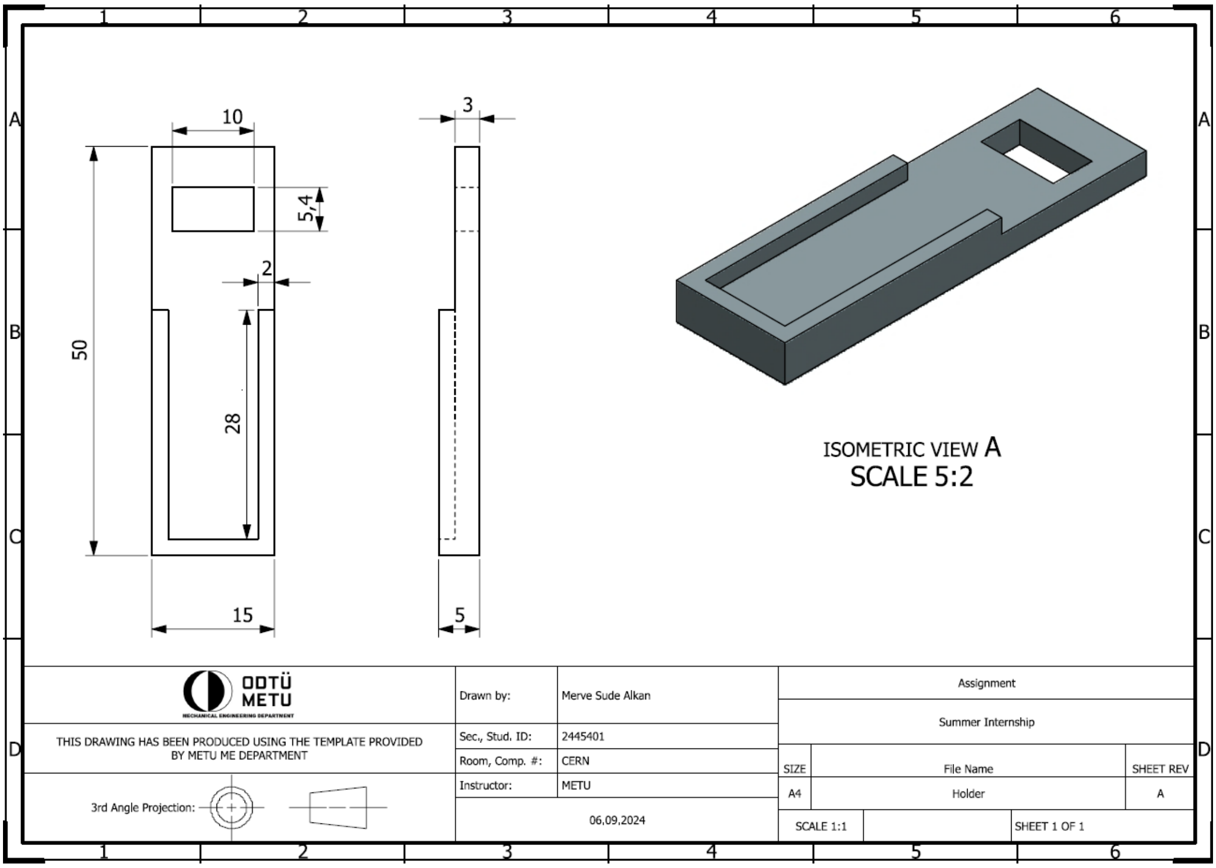

Figure 3.1: 3D Design of Holder

The barriers on the sides of the holders were added to prevent the liquid from impacting the edges too harshly during chemical experiments. The bottom wall was included to reduce convection and thus prevent deformation, as the lower parts of the chip tend to experience more deformation due to being closer to the heater during the experiments.

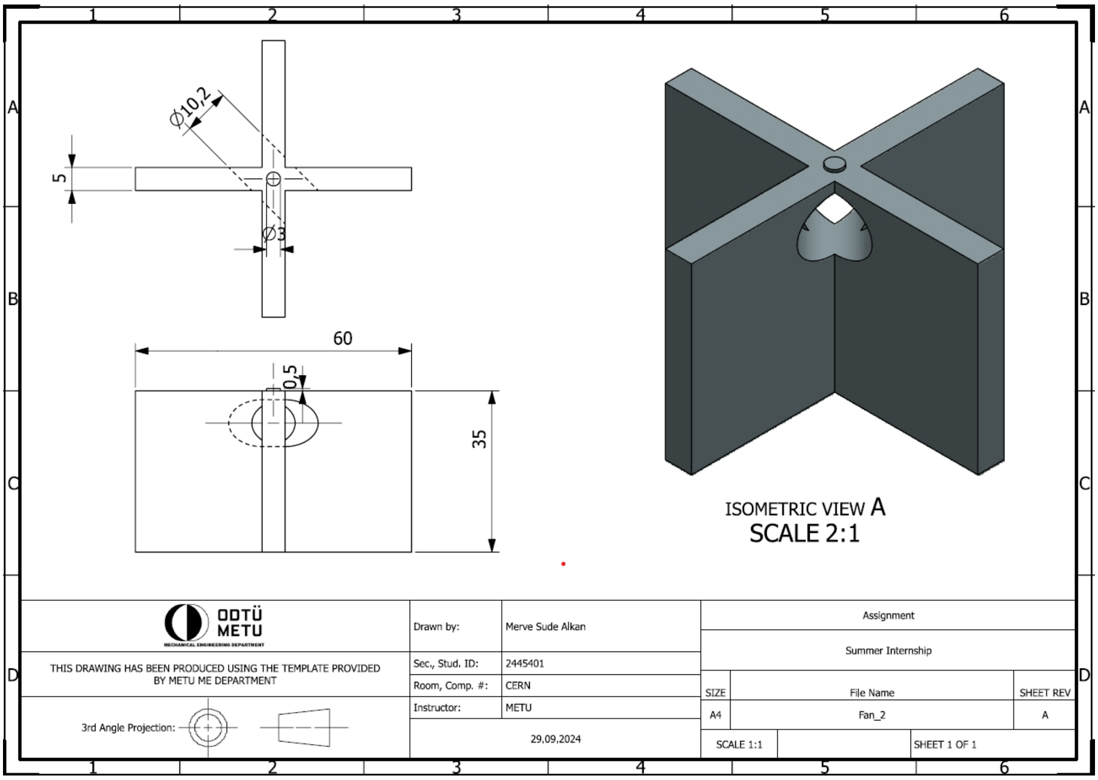

Figure 3.2: 3D Design of Fan_1

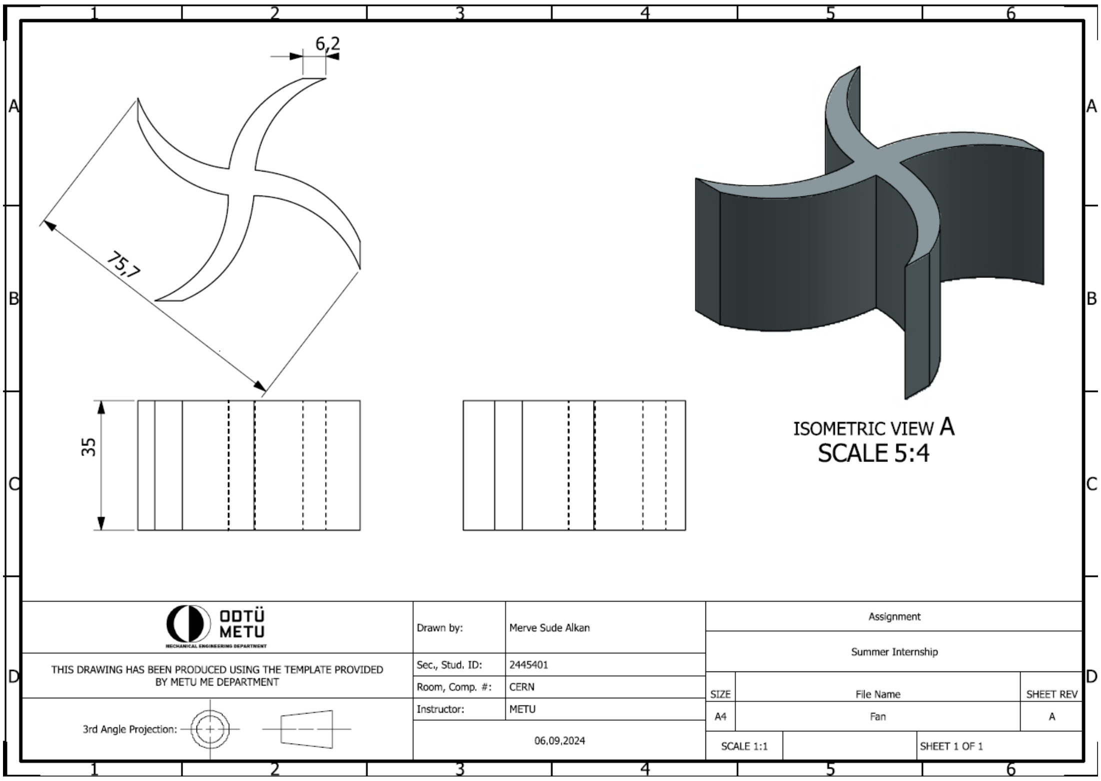

Figure 3.3: 3D Design of Fan_2

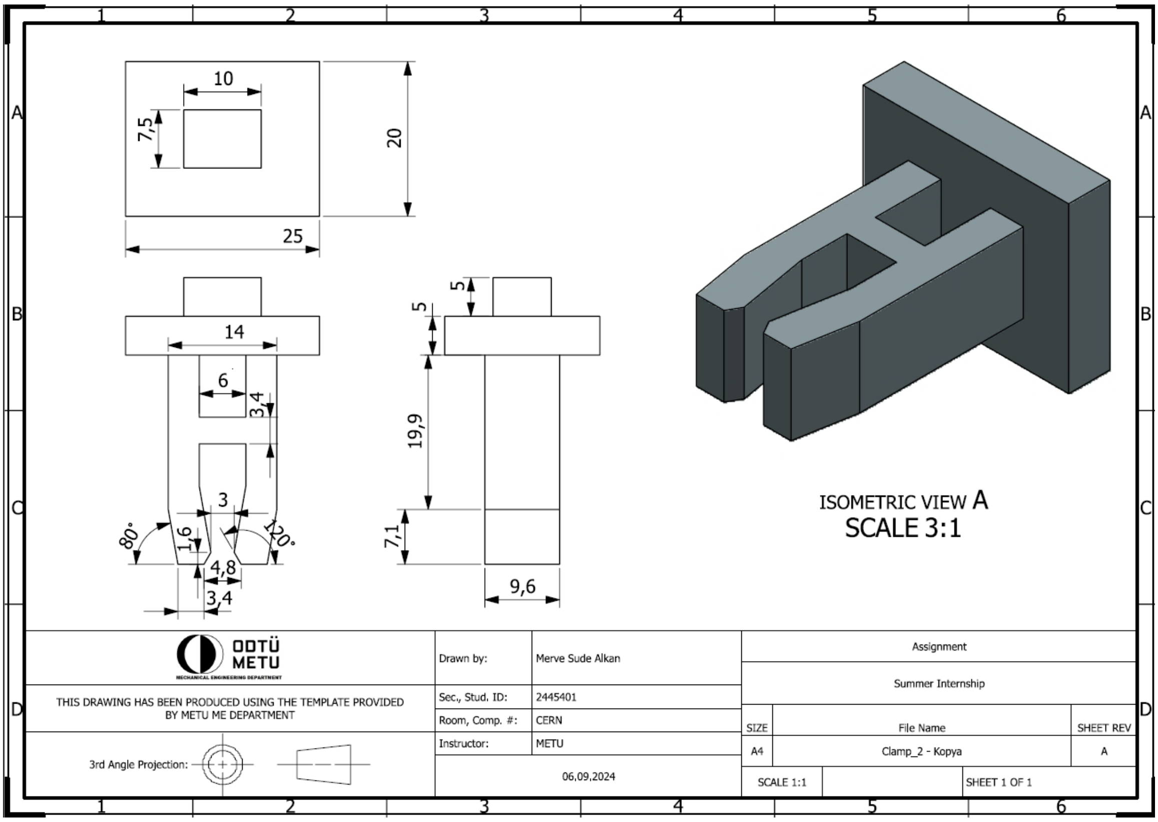

Figure 3.4: 3D Design of Clamp_1

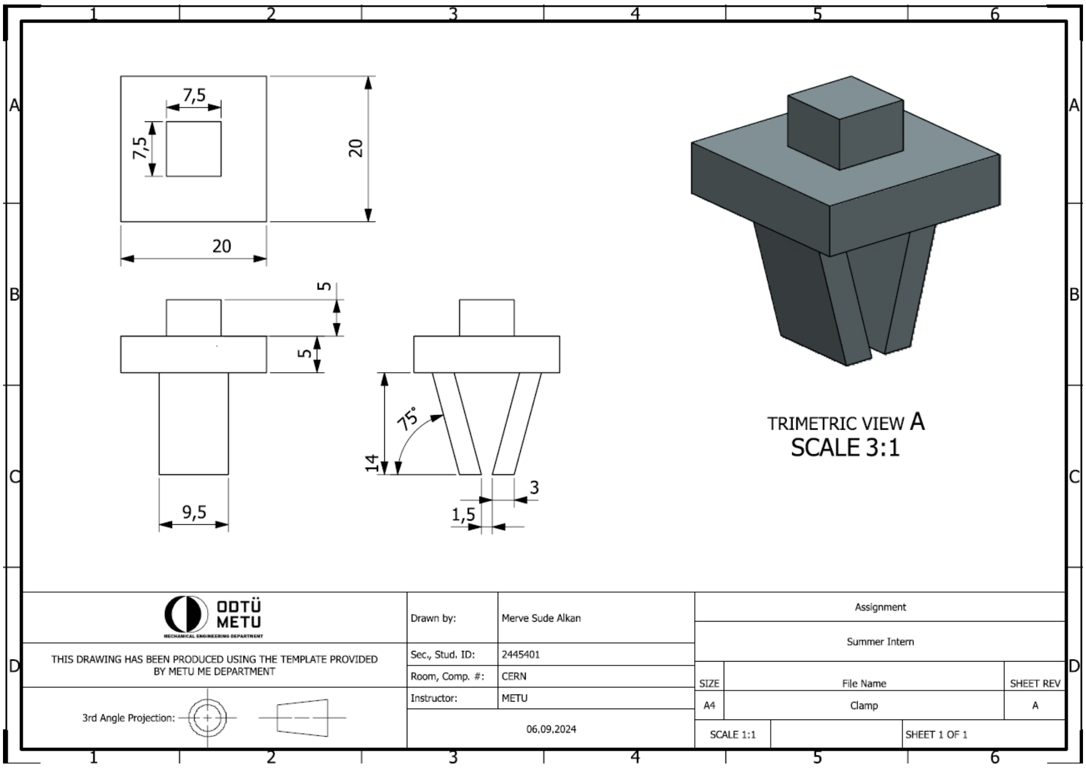

Figure 3.5: 3D Design of Clamp_2

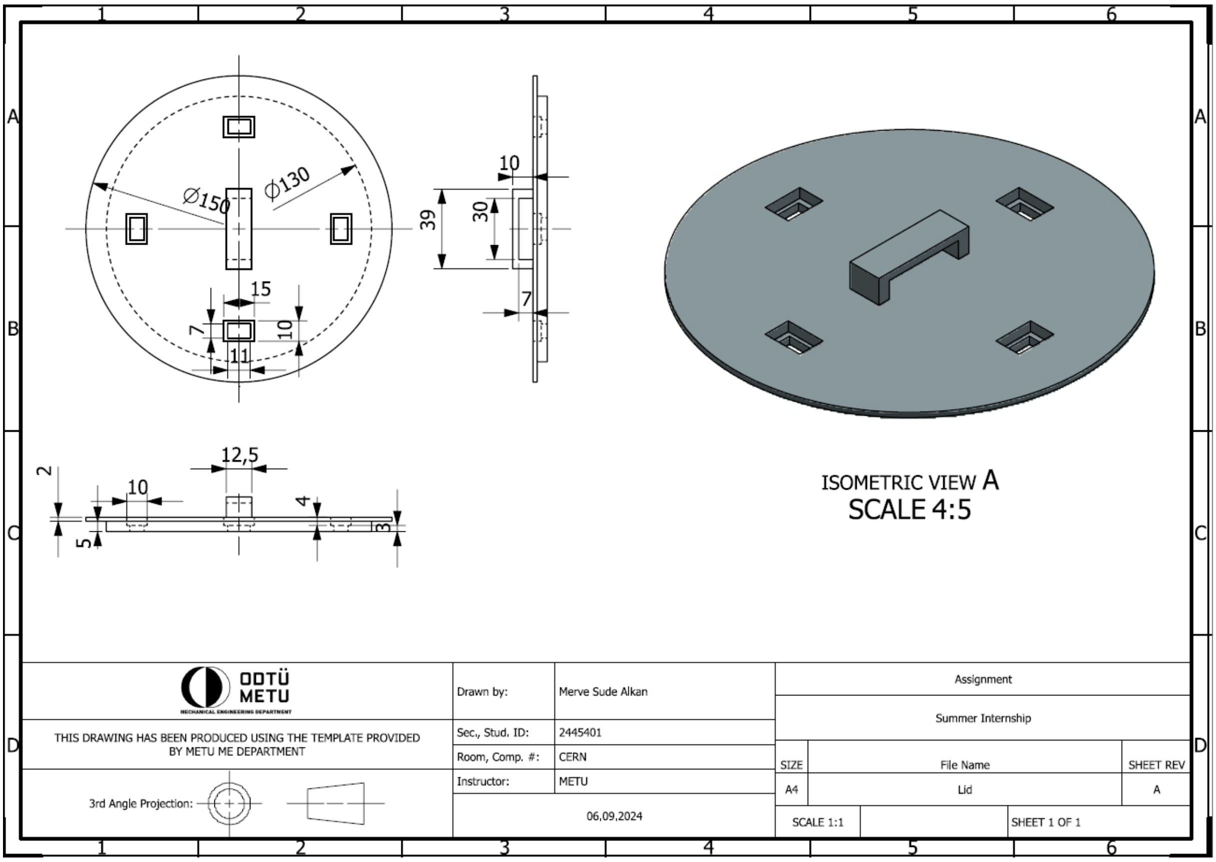

Figure 3.6: 3D Design of Lid

3.3 3D Printing

For 3D printing, Ultimaker S3 model 3D printing machine and its associated application were used. Unlike Prusa, this application allows for the selection of different infill pattern types, which enables the choice of stronger patterns. The strength of the material varies depending on the infill pattern type. For example, if more flexible materials are needed, the zig-zag pattern can be used. For the holders, the best option for low densities was the tri-hexagonal pattern, while the gyroid pattern was the most suitable for higher densities. These two pattern types significantly increase the material's strength.

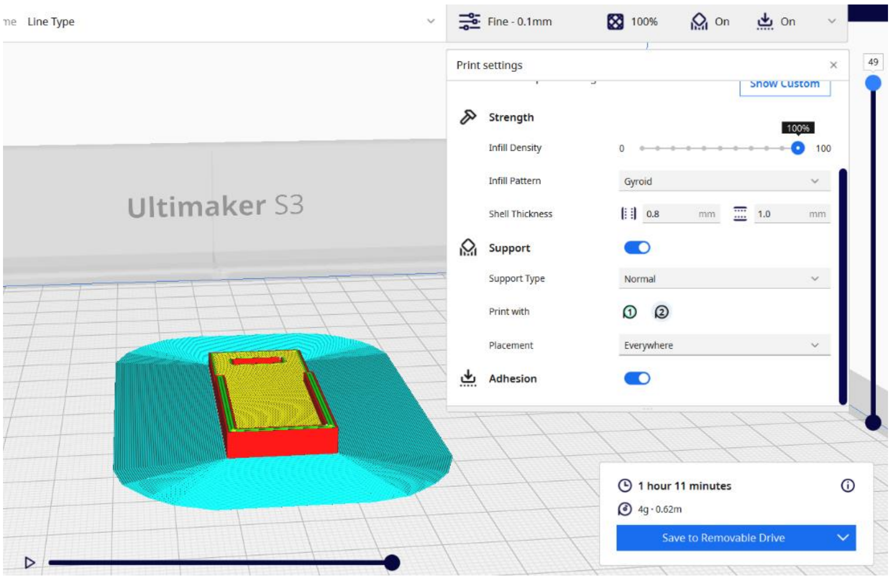

Figure 3.7: Preview of 3D Printing of Holder with Gyroid Pattern

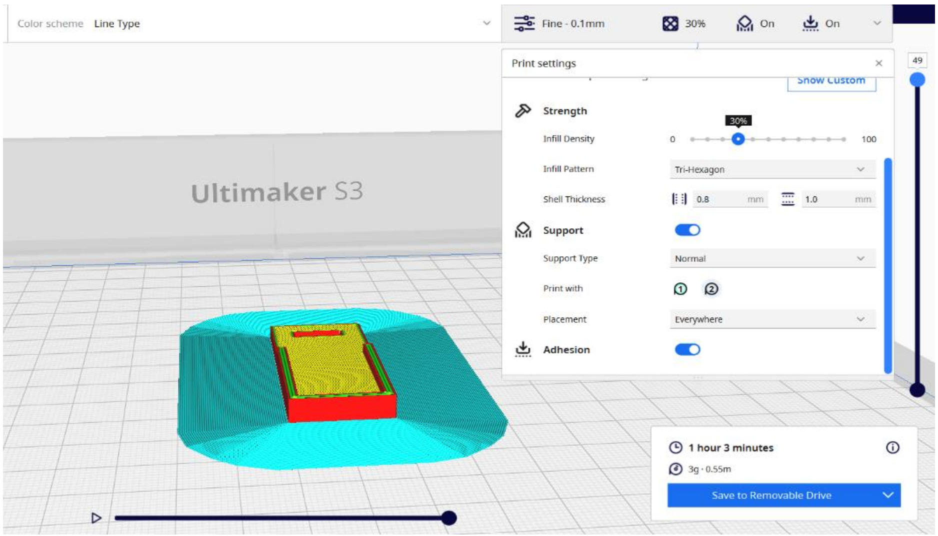

Figure 3.8: Preview of 3D Printing of Holder with Tri-Hexagonal Pattern

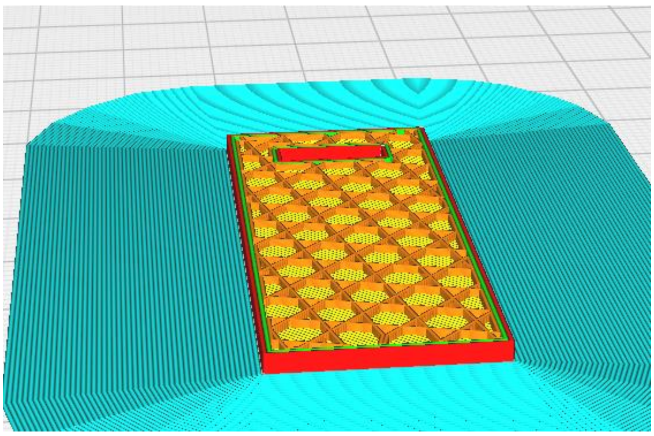

Figure 3.9: The inner design of Holder with Tri-Hexagonal Pattern

4. Conclusion

In this project, the optimization of the interconnection box was achieved, and its prototype was successfully produced. The significance and role of material type in 3D printing were understood, and the Prusa 3D printing machine was closely observed and its operation learned.

Heat transfer analysis was conducted for the nitrogen-carrying pipe, which transitions between two different temperatures inside the interconnection box, yielding various results. As a result of the analysis, it was concluded that the provided volumetric flow rate values were sufficient, and the required heat transfer was achieved. To prevent unnecessary heat generation, it is recommended to use a higher volumetric flow rate. The maximum usable volumetric flow rate was determined to be 5.5 L/s, and no further increase is possible since increasing the pipe's length would be required, but the pipe's maximum length cannot be extended further. The results are based on the assumption of linear temperature increase, so there are some discrepancies. The amount of heat supplied varies at each interval. As a continuation of the project, the next stage will involve maintaining a constant heat supply, experimenting with different values, and using trial and error to reach the actual solution.

Additionally, a holder, two clamps, two fans, and a lid were designed and 3D printed for use in ENIG plating. The use of the Ultimaker Cura 3D printing machine and its dedicated application were learned. Infill pattern options were explored, and the changes in material properties based on different patterns were observed. It was also learned how to create strong materials using minimal material.

5. References

[1] *NIST Chemistry Webbook, SRD 69*. Thermophysical Properties of Fluid Systems. (n.d.-a). https://webbook.nist.gov/chemistry/fluid/

[2] *Material properties: 304L stainless (UNS S30403)*. cryogenic material properties 304L Stainless. (n.d.). https://trc.nist.gov/cryogenics/materials/304LStainless/304LStainless_rev.htm

[3] Marghitu, D. B. (2001). *Mechanical Engineer's Handbook*. Academic Press.

[4] The Atlas Collaboration. (2020). *Technical design report: A high-granularity timing detector for the atlas phase-II upgrade*. CERN Document Server. (2020, June 5). https://cds.cern.ch/record/2719855?ln=en

[5] Volker, A., Schmidt, J. V., Dannheim, D., Svihra, P., Pinto, M. V. B., Oliveira, R. de, Braach, J., Yang, X., Ruat, M., Magalhaes, D., Vignali, M. C., Calderini, G., & Kristiansen, H. (n.d.). Pixel detector hybridisation and integration with anisotropic conductive adhesives. https://arxiv.org/html/2312.09883v2

Appendix

https://cernbox.cern.ch/s/oT31LQBCyu83U7V